https://doi.org/10.5194/egusphere-2026-11
Preprint. Discussion started: 30 January 2026

Flapping motion of onset aurora

Office Geophysik, Ogoori, 838-0141, Japan

Osuke Saka

osuke.saka001@gmail.com

Abstract

Onset aurora is meso-scale auroral forms (100s km) of spiral aurora arising out of the equatorward arc in association with the initial pulse of Pi2 pulsation, i.e., onset of field line dipolarization. Following the auroral onset, the head of the equatorward arc rapidly turns in a clockwise direction with expansion poleward, and during the second event of onset aurora, the whole of the arc rotates clockwise as viewed along the field lines. We model the deformation of onset aurora as an ExB drift of negatively charged solitary potential area (ion hole) in the polar ionosphere. It is suggested that twist motion of the onset aurora is analogous to the flapping motion of transmission belt in a factory driven by rotating line shaft. Like fluctuations in the line-of-sight velocity of the belt, non-uniform plasma flows in the ion hole trigger flapping motion of the arc.

1. Introduction

The onset aurora initiates with the initial pulse of Pi2 pulsation. Pi2 pulsations observed in very low latitude stations are geomagnetic micropulsation occurring in concert with global reconfiguration of the nightside magnetosphere at field line dipolarization, i.e., cavity oscillations. In contrast, high-latitude Pi2 pulsations are geomagnetic oscillations excited locally in auroral regions with the onset of field line dipolarization [Keiling and Takahashi, 2011 and references therein]. Possible location of peak power for the high-latitude Pi2s is suggested to be at the Harang Discontinuity (HD) [Rostoker and Samson, 1981; Samson and Rostoker, 1983]. The onset aurora is a meso-scale form of discrete aurora referred to as Westward Traveling Surge (WTS).

Two spiral types are reported for discrete auroras in the literature according to rotational direction when viewed along the field lines, counterclockwise (CCW) and clockwise (CW). However, opposite rotations in discrete aurora are not well understood [Haerendel, 2006].

https://doi.org/10.5194/egusphere-2026-11
Preprint. Discussion started: 30 January 2026

The former type (CCW) is caused by wave polarizations of current carrying Alfven waves generated in the magnetosphere by the plasma instability [Forsyth et al., 2020]. Or CCW rotations are generated in the ionosphere by shear flow instability of flux tubes containing upward field-aligned currents [Hallinan, 1976; Lysak and Song, 1996; Partamies et al., 2001; Keiling et al., 2009]. The ionosphere plays as secondary effects in the magnetosphere-ionosphere coupling [Sato and Iijima, 1979; Lyons, 1980; Amm and Fujii, 2008; Haerendel and Partamied, 2024]. The second type (CW) is called the S-aurora where auroral vorticities rotate in clockwise directions that are counter to the first type [Oguti, 1975]. The onset aurora showing the second type rotation is a meso-scale auroral form of S-aurora. In this report, we regarded auroral arc as negatively charged solitary area in the polar ionosphere or an "ion hole." Those ion holes are not solitary waves caused by plasma kinetics in the collisionless plasmas [Temerin et al., 1982; McFadden et al., 2003] but rather solitary structures generated in collisional ionosphere by precipitating energetic electrons. Although flow shears in the ion hole develop winding auroras of the first type with CCW rotations [Lysak and Song, 1996], we suggest flapping instability of the ion hole deforms the onset aurora with opposite sense of rotation.

Examples of the onset aurora are presented in section 2, pre-activated magnetosphere for the present aurora model is discussed in section 3, field-aligned currents in the pre-activated magnetosphere are shown in section 4, formation of ion hole in the polar ionosphere is in section 5, and flapping motion of the ion hole is discussed in section 6. As summarized in section 7 the deformation of onset aurora is identical to the flapping motion of ion hole.

2. Example of "onset aurora"

The first example of the onset aurora is presented in Figure 1 taken at Shamattawa (SHM), Canada on 02 Jan 1986. The spiral form shows clockwise turnover of the poleward arc splitting from the equatorward arc. Figure 2 presents a second example of the onset aurora taken at Shamattawa, Canada in 24 Jan 1986. This event demonstrates a clockwise twist with splitting arc at the poleward boundary, referred to as poleward boundary aurora surge [Saka et al., 2012]. Five events of the onset aurora from Saka et al., (2012, 2014) are examined. Four events demonstrate splitting type of the clockwise spirals (Figure 1) and one event is a rotational type of spirals (Figure 2). Rotational features observed in the onset aurora are common features of the S aurora [Oguti, 1975]. Onset aurora is a meso-scale auroral form of S aurora.

https://doi.org/10.5194/egusphere-2026-11
Preprint. Discussion started: 30 January 2026

3. Pre-activated magnetosphere

Let us assume that horizontal plasma flows in the ionosphere are caused by incident westward electric fields from the convection surge in the magnetosphere, and that they create charge separations in the polar ionosphere which are negative in lower latitudes and positive in higher latitudes [Saka, 2019]. Some trapped electrons above the negatively charged area in the polar ionosphere displace the mirror height of trapped electrons upward. This effect may leave positive charges (protons) immediately above the ionosphere creating an electron rich region in the magnetosphere. Negative charge effect constitutes charge separations along the field lines, which yields transient upward electric fields in the magnetosphere. In the flux tube where transient parallel electric fields exist, pitch angle distribution of electrons and ions cannot agree at any point of B. Parallel electric fields with disparate pitch angle distributions are a steady-state solution of the flux tube [Persson, 1963].

Meanwhile, some of trapped electrons above the positively charged area do not return to the magnetosphere because they were drawn into the ionosphere. The magnetosphere may become an electron void region. Negative charges immediately above the ionosphere and an electron void region in the magnetosphere initiate charge separation. Charge separation yields downward electric fields that are a steady-state solution of flux tubes. A pair of acceleration regions in the magnetosphere is produced by the ionosphere through ionospheric injection mechanism [Saka, 2023].

Electrostatic potential calculated from the steady-state upward parallel electric fields in Figure 6(A) is presented in Figure 3 from 0 km to 10000 km above the polar ionosphere. Resulting parallel ($T_{//}$) and perpendicular ($T_{\perp}$) temperatures in eV are calculated by

$$T_{//,\ \perp} = \frac{m_q}{2} \cdot \int_{\Sigma} v^2_{//,\ \perp} f(v,\phi) d^3 v \,. \qquad (1)$$

Integration occurs over the velocity space (Σ) occupied by the trapped electrons or ions. Here, $f(v,\phi)$ is the Maxwell distribution function for velocity distributions of ions and electrons with ϕ representing field line potential. The velocity distribution function of ions/electrons is given by,

$$f(v_{//}, v_{\perp}; \phi) = \left(\frac{m_q}{2\pi k T_q} \right)^{3/2} \exp\left(-\left(\frac{m_q}{2kT_q} (v_{//}^2 + v_{\perp}^2) + \frac{q|e|\phi}{kT_q} \right) \right). \qquad (2)$$

Here kT_q is ion/electron temperatures in eV. Potential ϕ is 0 volt at the ionosphere. In the case of upward electric fields, due to pitch angle disagreement between electrons and ions, perpendicular temperature anisotropy of electrons becomes larger, while for ions, parallel

https://doi.org/10.5194/egusphere-2026-11
Preprint. Discussion started: 30 January 2026

anisotropy becomes larger than the case without parallel potential (Figure 4). This relation reverses for the downward electric fields.

We suppose that the pre-activated magnetosphere develops perpendicular temperature anisotropies of plasma sheet electrons. However, auroras are yet to manifest. When anisotropies resolve for whatever reason by filling loss cone with plasma sheet electrons, auroras then initiate in the polar ionosphere.

4. Field-aligned currents

Ion drift carries Pedersen currents between complementary pair of field-aligned current regions. Ion drift ($\mathbf{u}_{i\perp}$) may be given as [Kelley, 1989],

$$\mathbf{u}_{i\perp} = \frac{\Omega_i}{B\nu_{in}} \mathbf{E}_p . \qquad (3)$$

Here, Ω_i, ν_{in}, $\mathbf{E}_p$ denote ion cyclotron frequency, ion-neutral collision frequency and polarization electric fields, respectively. By substituting mean ion cyclotron ($1.6\times10^2 s^{-1}$) and ion-neutral collision frequencies ($5.4\times10^3 s^{-1}$) in the ionosphere [e.g., Prince and Bostick, 1964; Tohmatsu, 1990], we have ion drift velocities on the order of 5.9×10^1 m/s for electric fields of the order of 0.1 V/m. Those drifting ions carry Pedersen currents of the order of $1.0 \mu A m^{-2}$ in the ionosphere ($n_i = 1.0\times10^{11} m^{-3}$). These ionospheric currents might be redirected to the field-aligned currents above the ionosphere.

We assume that plasmas are collisionless above 140 km in altitudes because both electron- and ion-gyrofrequencies exceed electron-neutral and ion-neutral collision frequencies, respectively [Rishbeth and Garriot, 1969]. Field-aligned currents above the ion hole are calculated by the following relation,

$$J_{//} = n|e|q\int_{\Sigma} v_{//} \cdot f(v,\phi) d^3v . \qquad (4)$$

Here, $f(v,\phi)$ is the Maxwell distribution function for velocity distributions of ions and electrons at different temperatures, ϕ representing field line potential. n denotes background density of electrons (q=-1) and ions (q=1). $|e|$ is the charge. Integration was carried out over the velocity space (Σ) occupied by the target particles [Chiu and Schulz, 1978].

Upward currents are carried in upward electric field regions by upgoing ionospheric

https://doi.org/10.5194/egusphere-2026-11
Preprint. Discussion started: 30 January 2026

ions as well as downgoing plasma sheet electrons. Ionospheric ions are carried in velocity space of loss cone modified by the parallel potential. Influence of ionospheric electrons on upward currents can be ignored because of the potential barrier to upgoing ionospheric electrons. Plasma sheet electrons are carried earthward through phase space trajectory passing through the loss cone modified by the potential, referred to as straight-through trajectory [Knight, 1973]. Altitude profiles of the upward electric fields and of upward current intensities for L=6 are presented in Figures 5(A) and 5(B), respectively. Altitude profile of the upward currents is shown from 231 km to 5005 km. Background ion density (n_i) is assumed to be $1.0\times10^{11}m^{-3}$. Ion current intensity at any point of B increases with increasing ion temperature (Ti=0.1eV, 1eV, and 10eV). Upon breakdown of the electron temperature anisotropy, plasma sheet electrons ($T_e = 1keV$, $n_e = 1.0\times10^{6}m^{-3}$) carry upward currents through the straight-through trajectories (black line in Figure 6(B)). Plasma sheet currents increase linearly with increasing potential (current-voltage relation). Downward currents are carried in downward electric field regions by upward moving ionospheric electrons. Ion contributions to downward currents can be ignored because of the potential barrier to upgoing ions. Contributions of downgoing plasma sheet ions through straight-through trajectory is not included. Upgoing electrons are carried in velocity space of loss cone modified by the parallel potential. Altitude profiles of the downward electric fields and of downward current along geomagnetic field line of L=6 are presented in Figures 6(A) and 6(B) respectively. Background electron density, n_e, is assumed to be $1.0\times10^{8}m^{-3}$. Current intensity at any point of B increases with increasing electron temperatures (Te=1.0eV, 10eV, 100eV, and 1keV).

Background cold plasma densities in downward current region are small as compared to those in upward current region. This difference may result from the fact that both ionospheric electrons and ions are subtracted upwards and equatorward, respectively, from downward current regions to satisfy quasi-neutrality of the ionospheric plasmas. Downward current regions would form an “auroral ionospheric cavity” [Doe et al., 1993].

5. Ion hole formation

We consider that a solitary area with negative potential is created in the polar ionosphere by auroral precipitations in association with breakdown of the temperature anisotropies in the pre-activated magnetosphere. Stop altitudes of the incident energetic electrons (2 - 10keV) range from 100km to 150km, where green (O; 557.7 nm) and blue (N_2^+; 427.8 nm) emission

https://doi.org/10.5194/egusphere-2026-11
Preprint. Discussion started: 30 January 2026

lines are activated with lifetimes of 0.7s and $70\mu s$, respectively [Oguti, 2010; Tohmatsu, 1990]. The stop altitudes also correspond to a thin layer of collisional ions and collisionless electrons referred to as an ionosphere [Rishbeth and Garriot, 1969]. At this stop altitude, incident energetic electrons produce negatively charged potentials composed of secondary electrons (100 eV). The potential barriers inhibit free escape of secondary electrons. Ionospheric ions escape outward as ion outflows but are accumulated horizontally to confine secondary electrons as electron rich area. The ion hole is generated in the polar ionosphere, where electron populations (primary and secondary) are greater at the inside than at the rim. Electron populations initially peaked at the center may spread horizontally outward to the rim. Consequently, electric fields show peak amplitudes at the rim with null amplitudes within the hole. This causes a decrease of free energy *U* of the ion hole which can be written as,

$$U = \frac{\varepsilon_0}{2} \iint \left(E_x^2 + E_y^2 \right) dxdy . \qquad (5)$$

Here, ε_0 is dielectric constant in vacuum, and E_x, E_y are electric field component in horizontal plane. Maximum size of null amplitude regions may be determined by balance of ionization rate and recombination loss in the ion hole. Resulting 2D profiles of ion hole potential, charge separation (n_i-n_e), and electric field amplitude are shown in Figure 7. Applying ionospheric injection scenario to the ion hole, we can expect downward FACs peaked at the rim and upward FACs at the inside.

6. Twist motion of ion hole

In the ion hole, it is suggested that plasma flows at the outer boundary develop Kelvin-Helmholtz (KH) instability that initiates windup deformation of the auroral arc in CCW directions [Hallinan, 1976; Lysak and Song, 1996; Keiling et al., 2009]. In this report, however, we discuss deformation of the onset aurora in CW directions in terms of flapping instability of the auroral arc, triggered by non-uniform plasma flows in the ion hole.

Figure 8 shows 2D distribution of ion hole potential $\phi(x,y)$ in X-Y plane as well as ExB drift of ionospheric electrons in the ion hole. We assume ion hole potential in sheet-like structures narrowing in Y direction. Potential is assumed to be null $\phi(x,y)=0$ outside of the ion hole. Potential profiles along Y component are presented at five different locations in X. In Figure 8(A), electric fields show peak amplitudes at the rim with null amplitudes within the hole. Ionospheric electrons flow along the rim in the clockwise directions as demonstrated in Figure 8(B) by black arrows. In the ion hole, electron flows are divided into six closed circles with the same flow speeds. When converging electric field areas expand

https://doi.org/10.5194/egusphere-2026-11
Preprint. Discussion started: 30 January 2026

within the ion hole (Figure 8(C)), drift speeds of ionospheric electrons at the rim decrease moving away from the center (Figure 8(D)). Electrons drift along the rim at the velocity $E_y(x)/B$. Here, $E_y(x)$ is calculated from $\pm\phi(x,0)/L$. $\phi(x,0)$ is ion hole potential along the X-axis, referred to as principal axis hereafter. L is characteristic distance of potential drop along minor axis of the sheet (Y-axis). Non-uniform drifts along the rim turn to perpendicular drifts ($V_y(x)$) as illustrated in Figure 8(D) by red arrows. These perpendicular flows twist the principal axis of the ion hole because there is no return flow channels closed in the ion hole (Flapping instability).

The $V_y(x)$ can be written as,

$$V_y(x) = \frac{1}{B}\left(\frac{\phi(x+\Delta x/2,0)}{L} - \frac{\phi(x-\Delta x/2,0)}{L}\right). \qquad (6)$$

Equation 6 is approximated as,

$$\frac{1}{L \cdot B}\frac{d\phi(x,0)}{dx}\Delta x. \qquad (7)$$

Here, B denotes field magnitudes in the ionosphere, Δx is separation distance of the drift circles, and $d\phi(x,0)/dx$ denotes converging electric fields along the principal axis, $E_x(x)$. When $2 \cdot L = \Delta x$, residual flows ($V_y(x)$) can be given by $2 \cdot \left(E_x(x) \times \tilde{B}/B\right)$. $\tilde{B}$ is unit vector of B. Electric field drift of the principal axis ($E_x(x)/B$) can be used as a proxy of ion hole twist.

The ExB drift is determined simply by distribution of charged particles along the principal axis. Charge distributions are shown in Figure 9 highlighted by an ion rich region ($\Delta n>0$, $\Delta n=n_i-n_e$) and electron rich region ($\Delta n<0$). Let us assume that electron rich areas are initially peaked at the center, X=0 (Type 1, not shown). In the following steps, electron rich areas fill the middle of the X-axis and they eventually spread to the edge of the arc (Type 2 and Type 3 in Figure 9), because free energy of the ion hole decreases from Type 1 to Type 2 and to Type 3. For Type 3, polarity of converging electric fields is separated in X, positive polarity (electric field vectors point towards positive X) in $-1.5<X<-1.0$ and negative polarity (electric field vectors point to negative X) in $1.0<X<1.5$. Motion of the electron rich region ($\Delta n<0$) is examined to simulate auroral motion. Continuous electron precipitations are assumed as well at the electron rich area. The results are shown in the bottom panel of Figure 9. For Type 2, arc alignment rotates clockwise at the center. For Type 3, clockwise rotation

https://doi.org/10.5194/egusphere-2026-11
Preprint. Discussion started: 30 January 2026

occurred at the edge of the arc, $-1.5<X<-1.0$ and $1.0<X<1.5$, resulting in clockwise splitting of the arc. Deformation of principal axis for Type 2 corresponds to clockwise twist of the onset aurora presented in Figure 2. Type 3 corresponds to clockwise turnover of the onset aurora shown in Figure 1 and to splitting motion of S aurora referred to as "peeling-off" [Oguti, 1981].

7. Summary

Deformations of the onset aurora can be considered twist motions of auroral arc in the polar ionosphere due to flapping instability of the ion hole. When a sheet-like ion hole merges with a polar cap convection pattern, the ion hole forms Harang Discontinuity (HD) in the midnight sector. Westward expansion of the western edge of the ion hole due to longitudinal expansion of field line dipolarization corresponds to Westward Traveling Surge [Fujii et al., 1994; Lyons et al., 2013; Saka and Hayashi, 2017]. The onset aurora is located at source location of Pi2 pulsations in the polar ionosphere. At this location, excess charges accumulated by transverse electric fields are released as injections out of the ionosphere to ensure quasi-neutrality of ionospheric plasmas. To facilitate the injection of the ionospheric plasmas, parallel electric fields develop there by charge separations along the geomagnetic field lines. Those internal processes of the polar ionosphere at the Pi2 source region would result in auroral drivers of the onset aurora.

8. Acknowledgements

The author acknowledges Nozomu Nishitani for valuable advice and perspective. Thanks also to anonymous referees for their critical comments and suggestions.

9. Data availability

Data used in Figures 1 and 2 are adapted from Saka et al., 2012. Those are available upon request to Osuke Saka (osuke.saka001@gmail.com).

10. Competing interest

The author declares that there is no conflict of interest.

References

Amm, O. and Fujii, R.: Separation of cowling channel and local current closure currents in the vicinity of a substorm break up spiral, J. Geophys. Res., 113, A06304, doi:10.1029/2008JA013021, 2008.

Chiu, Y.T., and Schulz, M.: Self-consistent particle and parallel electrostatic field distributions in the magnetospheric-ionospheric auroral region, J. Geophys. Res., 83, 629-642, 1978.

Doe, R.A., Mendillo, M., Vickrey, J.F., Zanetti, L.J., and Eastes, R.W.: Observations of nightside auroral cavities, J. Geophys. Res., 98, 293-310, 1993.

Forsyth, C., Sergeev, V.A., Henderson, M.G., Nishimura, Y. and Gallardo-Lacourt, B.: Physical processes of meso-scale, dynamic auroral forms, Space Sci. Rev., 216:46, https://doi.org/10.1007/s11214-020-00665-y, 2020.

Fujii, R., Hoffman, R.A., Anderson, P.C., Craven, J.D., Sugiura, M., Frank, L.A. and Maynard, N.C.: Electrodynamic parameters in the nighttime sector during auroral substorms, J. Geophys. Res., 99, 6093-6112, 1994.

Haerendel, G.: The enigma of auroral spirals, Abstract presented in COSPAR, 2006.

Haerendel, G. and Partamies, N.: On the formation of auroral spirals, J. Geophys. Res. Space Physics, 129, e2024JA032413. https://doi.org/10.1029/2024JA032413, 2024.

Hallinan, T.J.: Auroral spirals 2. Theory, J. Geophys. Res., 81, 3959-3965, 1976.

Keiling, A., Angelopoulos, V., Weygand, J.M., Amm, O., Spanswick, E., Donovan, E., Mende, S. McFadden, J., Larson, D., Glassmeier, K-.H. and Auster H.U.: THEMIS ground-space observations during the development of auroral spirals, Ann. Geophys., 27, 4317-432, 2009.

Keiling, A. and Takahashi, K., Review of Pi2 models, Space Sci. Rev., 161, 63-148, 2011.

Kelley, M.C.: The earth's ionosphere: plasma physics and electrodynamics, Academic Press, Inc., 1989.

Knight, S.: Parallel electric fields, Planet. Space. Sci., 21, 741-750, 1973.

Lyons, L.R.: Generation of large-scale region of auroral currents, electric potentials, and precipitation by the divergence of the convection electric field, J. Geophys. Res., 85, 17-24,1980.

Lyons, L.R., Nishimura, Y., Gallardo-Lacourt, B., Zou, Y., Donovan, E., Mende, S., Angelopoulos, V., Ruohoniemi, J.M. and McWilliams, K.: Westward traveling surges:

https://doi.org/10.5194/egusphere-2026-11
Preprint. Discussion started: 30 January 2026

sliding along boundary arcs and distinction from onset arc brightening, J. Geophys. Res., Space Physics, 118, 7643-7653, doi:10.1002/2013JA019334, 2013.

Lysak, R.L., and Song, Y.: Coupling of Kelvin-Helmholtz and current sheet instabilities to the ionosphere: A dynamic theory of auroral spirals, J. Geophys. Res., 101, 15411-15422, 1996.

McFadden, J.P., Carlson, C.W., Ergun, R.E., Mozer, F.S., Muschietti, L., Roth, I. and Moebius, E.: FAST observations of ion solitary waves, J. Geophys. Res., 108, doi:10.1029/2002JA009485, 2003.

Oguti, T.: Metamorphoses of aurora, Memoirs of NIPR, series A, 12, 1975.

Oguti, T.: TV observations of auroral arcs, Geophysical Monograph Series, Vol 25, 31-41, 1981.

Oguti, T.: Introduction to auroral physics (in Japanese), Edited by Nozomu Nishitani, Solar-Terrestrial Environment Laboratory, Nagoya University, 2010.

Partamies, N., Freeman, M.P. and Kauristie, K.: On the winding of auroral spirals: Interhemispheric observations and Hallinan's theory revisited, J. Geophys. Res., 106, 28913-28924, 2001.

Persson, H.: Electric field along a magnetic line of force in a low-density plasma: Phys. Fluids, 6, 1756-1759, 1963.

Prince, Jr., C.E. and Bostick, Jr., F.X.: Ionospheric transmission of transversely propagated plane waves at micropulsation frequencies and theoretical power spectrums, J. Geophys. Res., 69, 3213-334, 1964.

Rostoker, G. and Samson, J.C.: Polarization characteristics of Pi2 pulsations and implications for their source mechanisms: Location of source regions with respect to the auroral electrojets, Planet. Space Sci., 29, 225-247, 1981.

Rishbeth, H. and Garriott, O.K.: Introduction to ionospheric physics, International Geophysics, 14, 1-331, 1969.

Saka, O., Hayashi, K. and Koga, D.: Periodic aurora surge propagating eastward/westward at poleward boundary of aurora zone during the first 10 min intervals of Pi2 onset. J. Atomos. Solar Terr. Phys., 80, 285, 2012.

Saka, O., Hayashi, K. and Thomsen, M.: Pre-onset auroral signatures and subsequent development of substorm auroras: A development of ionospheric loop currents at the onset latitudes. Ann. Geophys., 32, 1011, 2014.

Saka, O. and Hayashi, K.: Longitudinal expansion of field line dipolarization, J. Atmos. Solar Terr. Phys., 164, 235-242, 2017.

Saka, O.: A new scenario applying traffic flow analogy to poleward expansion of auroras, Ann. Geophys., 37, 381-387, 2019.

https://doi.org/10.5194/egusphere-2026-11
Preprint. Discussion started: 30 January 2026

Saka, O.: Parallel electric fields produced by ionospheric injection, Ann Geophys., 41, 369-373, 2023.

Samson, J.C. and Rostoker, G.: Polarization characteristics of Pi2 pulsations and implications for their source mechanisms: Influence of the westward traveling surge, Planet. Space Sci., 31, 435-458, 1983.

Sato, T. and Iijima, T.: Primary sources of large-scale Birkeland currents, Space Sci. Rev., 24, 347-366, 1979.

Temerin, M., Cerny, K., Lotko, W. and Mozer, F.S.: Observations of double layers and solitary waves in the auroral plasma, Phys. Rew. Lett., 48, 1175-1179, 1982.

Tohmatsu, T.: Compendium of aeronomy, Published by TERRAPUB, Tokyo, 1990.

https://doi.org/10.5194/egusphere-2026-11
Preprint. Discussion started: 30 January 2026

Figure Captions

Figure 1

(A): 10-min plots from 0325:00 UT for 02 January 1986, showing a keogram along geomagnetic meridian passing SHM (66.3N, 336.0 in corrected geomagnetic coordinates). (B): H component of HUA at dip-equator (1.0N, 355.5 in geomagnetic coordinates), and (C): Inclination angle of field lines at geosynchronous satellite GOES 5 (footprint of this satellite is 64.0N, 349.8 in geomagnetic coordinates). Initial pulse of Pi 2 pulsations and associated dipolarization onset at 0328:30 UT is marked by vertical bar in red. All-sky images in the bottom are viewed from above the ionosphere (along the field lines). Poleward expansion of the onset aurora showing clockwise turnover of the splitting arc is demonstrated in consecutive images at 0328:30 and 0329:00. The auroral animation for 1 min intervals starting at 0328:00 can be found in supplementary material, 0102(1986).mp4.

Figure 2

Same as Figure 1 but auroral event from 0440:00 UT for 24 January 1986. Spiral form of the onset aurora shows clockwise rotation with splitting arc at the poleward boundary. Arc splitting starts at 0444:00 and clockwise rotation is demonstrated in the following images at 0444:30 and 0445:00. The auroral animation for 2 min intervals starting at 0443:00 can be found in supplementary material, 0124(1986).mp4.

Figure 3

Altitude profile of steady-state parallel potentials above the ionosphere. This potential profile, obtained by integrating upward electric fields in Figure 5(A), is sustained by the temperature anisotropies shown in Figure 4.

Figure 4

Altitude profiles of temperature anisotropy ($T_{\perp}/T_{//}$) for electrons and ions trapped in the mirror geometry, with parallel potentials (blue for electrons and orange for ions) and with no parallel potentials (gray). Geomagnetic field line of L=6 is selected to calculate the temperature anisotropy. Temperature of the trapped particles is 1 keV.

https://doi.org/10.5194/egusphere-2026-11
Preprint. Discussion started: 30 January 2026

Figure 5

(A): Altitude profiles of the upward electric fields in $\mu V/m$. (B): Upward current in $\mu A/m^2$ carried by ionospheric ions (O^+). Ion current intensity at any point of B increases with increasing ion temperature (Ti=0.1eV, 1eV, and 10eV). Upward electric fields in (A) are calculated from charge separations, positive immediately above the ionosphere and negative in the magnetosphere, due to negatively charged area in the polar ionosphere [Saka, 2023]. Plasma sheet electrons ($T_e = 1keV$) carry upward currents through the straight-through trajectories (black line). Straight-through trajectory denotes phase space trajectory of plasma sheet electrons going downward through the loss cone.

Figure 6

(A): Same as Figure 5 but for downward electric fields. (B): Downward electron currents at any point of B increase with electron temperature (Te=1.0eV, 10eV, 100eV, and 1keV). Downward electric field in (A) is calculated from charge separations, negative immediately above the ionosphere and positive in the magnetosphere, due to positively charged area in the polar ionosphere.

Figure 7

(A): Electrostatic potential of ion hole in X-Y plane. (B): Charge separation n_i-n_e in ion hole potential; n_i-n_e>0 (ion rich) at the rim, and n_i-n_e<0 (electron rich) at the inside. Number densities n_i, and n_e are ionospheric plasma density for ions and electrons, including secondary electrons. (C): Electric field amplitudes in ion hole. Electric fields are null in the ion hole. Converging electric fields peak along the outer boundary of the ion hole. Figures are viewed from above the ionosphere.

Figure 8

(A): A 2D distribution of ion hole potential $\phi(x, y)$ for sheet-like ion hole. A sharp gradient of the ion hole potential (converging electric fields) can be seen only at the outer boundary. (B): Flow of ionospheric electrons in the ion hole viewed along the field lines. Electron flows exist only at the outer boundary of sheet, which are shown by a closed trajectory in the direction of ExB drift (black arrows). The sheet-like ion hole is separated as six circles in X. There appeared no residuals in the electron drifts. (C): Same as (A) but ion hole potential

https://doi.org/10.5194/egusphere-2026-11
Preprint. Discussion started: 30 January 2026

has minimum peaks at the center. (D): Potential gradient in X breaks sheet-like ion hole into six circles with varying intensities. Varying intensities are depicted by thick and thin circles. Residual flows perpendicular to the X-axis are generated at the overlapping portion of the circle as shown by solid arrows in red. The residual flows closing in the ion hole twist the principal axis because there are no channels enabling return.

Figure 9

(Top): Distribution of n_i-n_e along the principal axis. Electron rich area is highlighted in gray. Ion rich area in orange. Two types of charge distributions are shown, Type 2 and Type 3. (Middle): Electric field profiles along the principal axis for Type 2, and Type 3. The electron rich area is delineated by dashed lines, where electric field vector marked in red points to the center (converging electric fields). (Bottom): Rotation of principal axis caused by positive E polarity are in a clockwise direction from 1 to 7, while for negative E polarity, axis rotations are in the same direction from -1 to -7.

https://doi.org/10.5194/egusphere-2026-11
Preprint. Discussion started: 30 January 2026

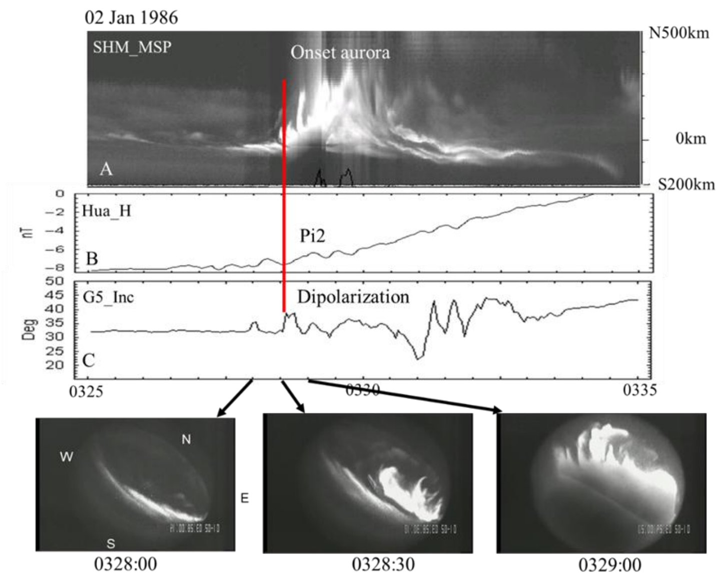

Figure 1

https://doi.org/10.5194/egusphere-2026-11
Preprint. Discussion started: 30 January 2026

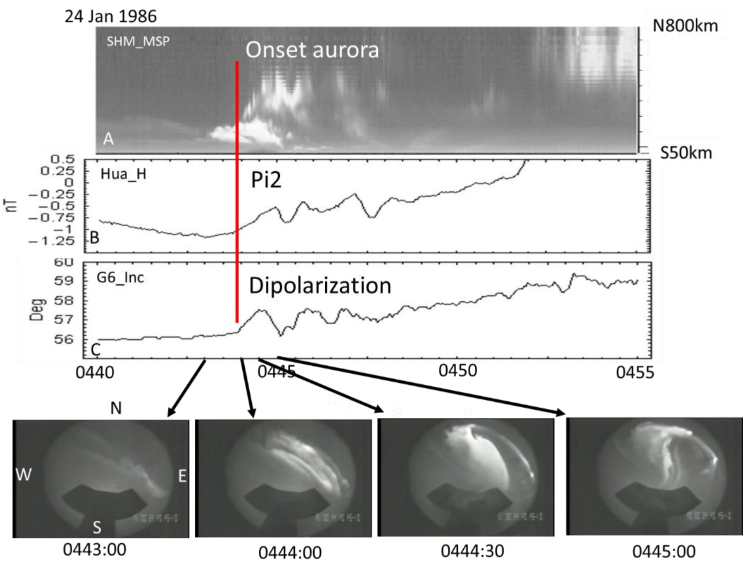

Figure 2

https://doi.org/10.5194/egusphere-2026-11
Preprint. Discussion started: 30 January 2026

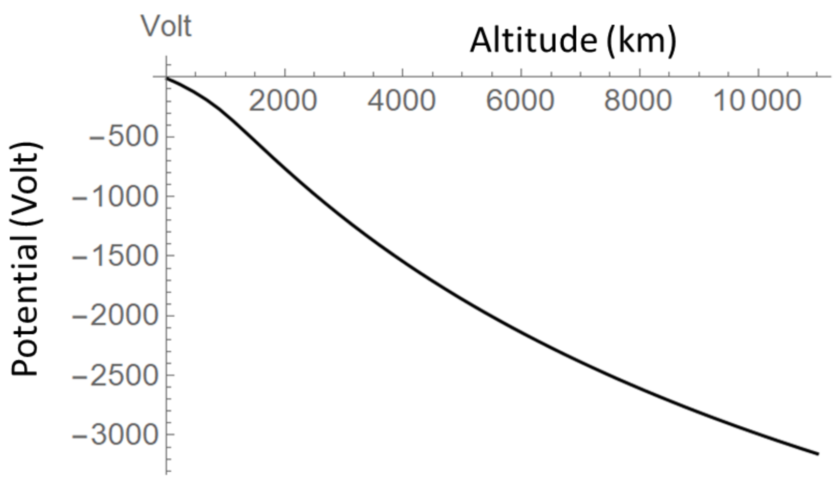

Figure 3

https://doi.org/10.5194/egusphere-2026-11
Preprint. Discussion started: 30 January 2026

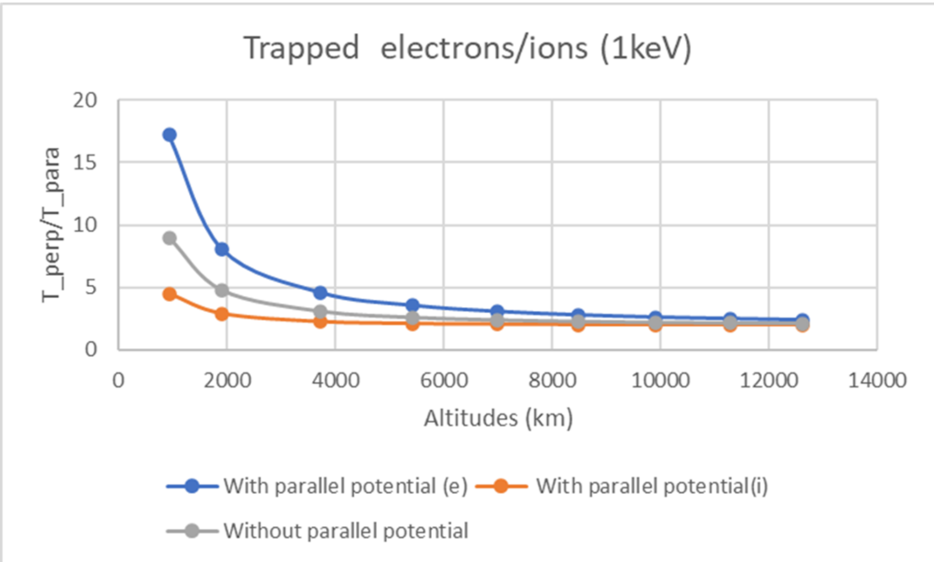

Figure 4

https://doi.org/10.5194/egusphere-2026-11
Preprint. Discussion started: 30 January 2026

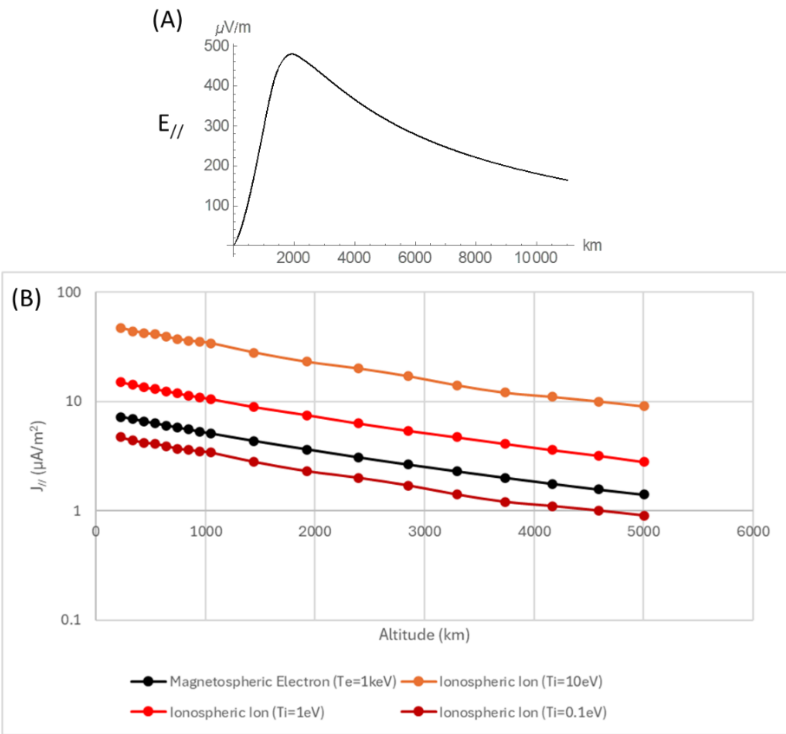

Figure 5

https://doi.org/10.5194/egusphere-2026-11
Preprint. Discussion started: 30 January 2026

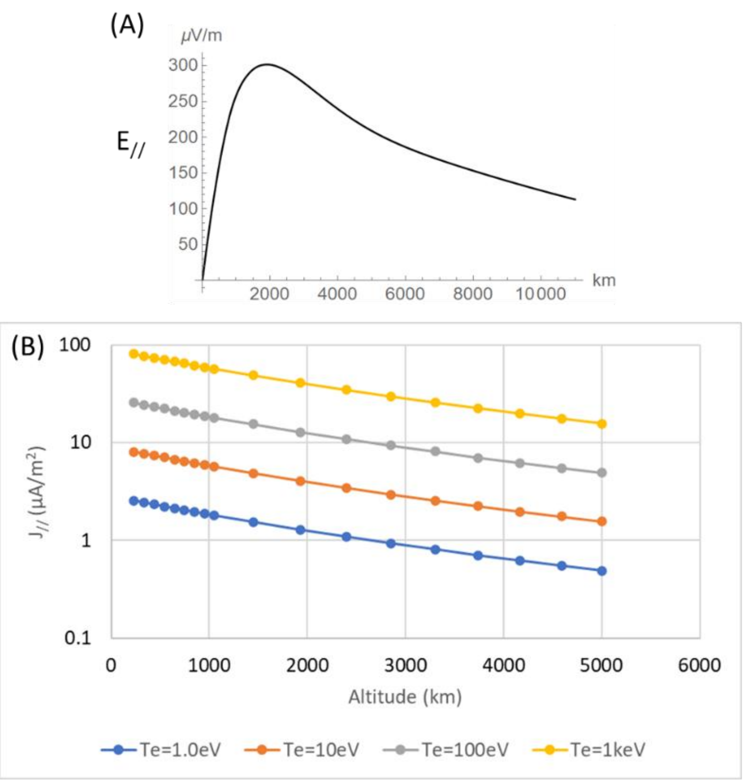

Figure 6

https://doi.org/10.5194/egusphere-2026-11
Preprint. Discussion started: 30 January 2026

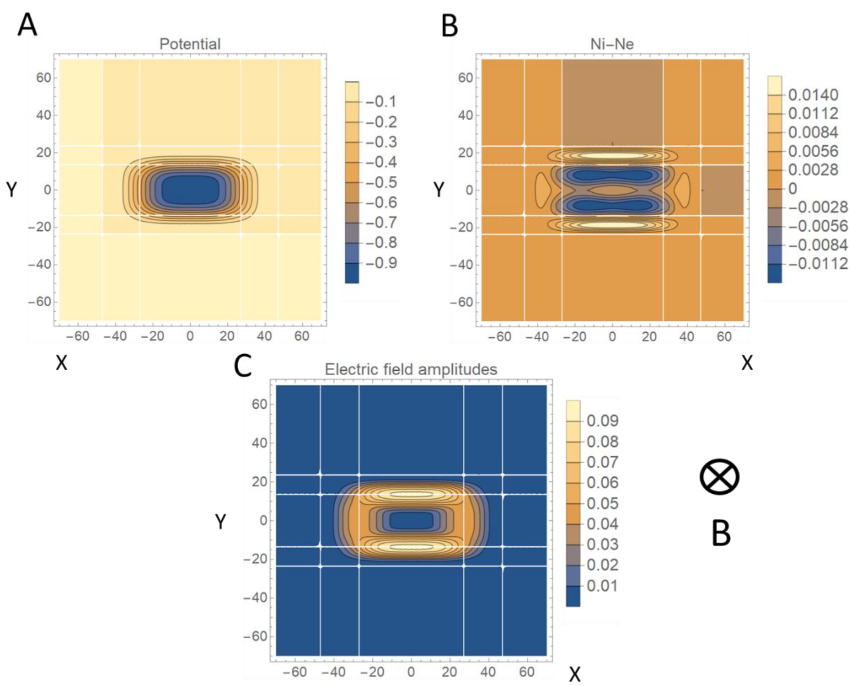

Figure 7

https://doi.org/10.5194/egusphere-2026-11
Preprint. Discussion started: 30 January 2026

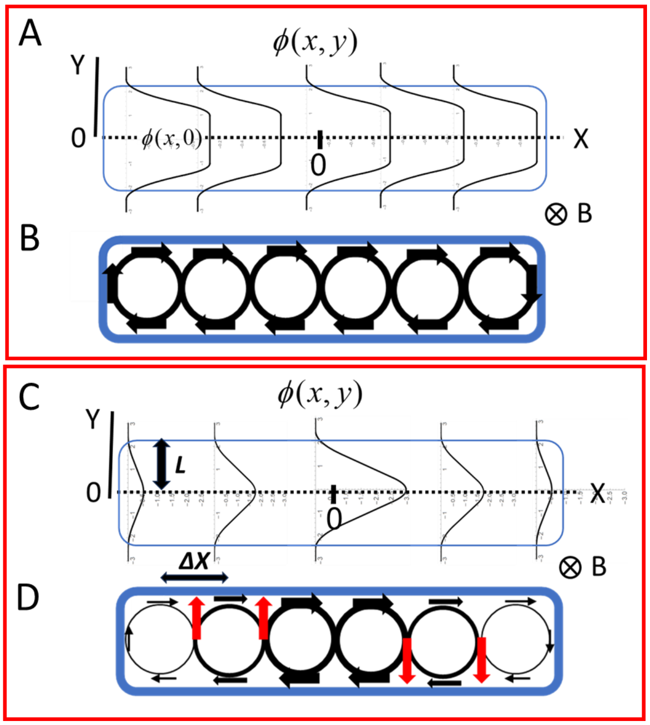

Figure 8

https://doi.org/10.5194/egusphere-2026-11
Preprint. Discussion started: 30 January 2026

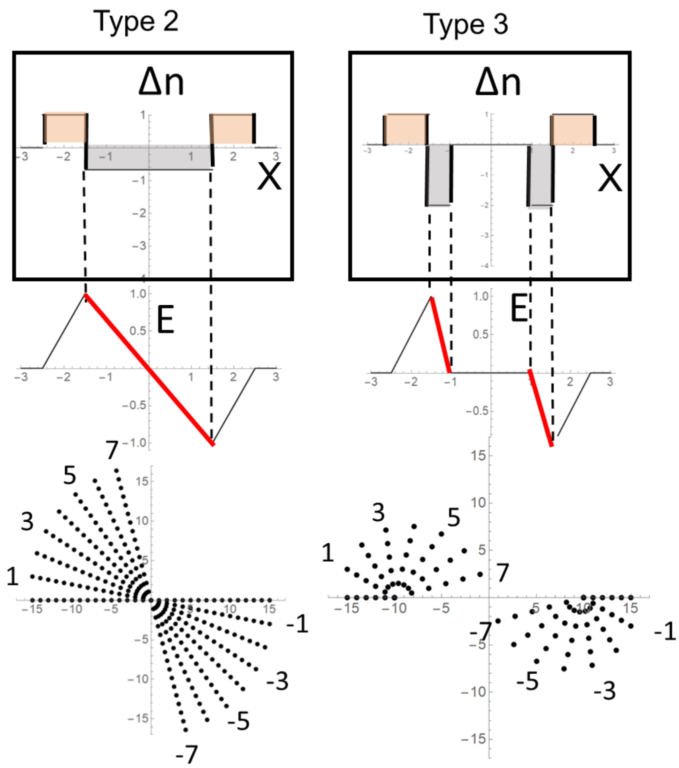

Figure 9